Sensor and Simulation Notes

Note 438

November 1999

Optimization of the Feed Impedance for an Arbitrary Crossed-Feed-Arm Impulse Radiating Antenna

J. Scott Tyo

Department of Electrical and Computer Engineering, US Naval Postgraduate School, Monterey, CA 93943

ABSTRACT

This note considers the optimization of feed arm geometry of 4-arm, coplanar plate IRAs when the angular position and extent of the arms are taken as free parameters. Previously, optimization of this class of antenna considered only the symmetric case where the two pairs of crossed feed arms were perpendicular to each other. Comparison is made using the prompt aperture efficiency, and the results indicate that the efficiency of 4-arm IRAs can be increased from ~25% for the perpendicularly crossed arms to ~35% for the optimum configuration. In addition to the optimization, the feed impedance of coplanar feeds is presented for general values of feed arm angle and plate width, and the optimum feed impedance is computed for each feed arm angle. The results in this note can be used to design the optimal 4-arm IRA with an arbitrary specified input impedance.

I. Introduction

Impulse radiating antennas (IRAs) are members of a class of antennas that are designed for the radiation of ultra-wideband (UWB) electromagnetic impulses. These antennas are perhaps better characterized as dispersionless, high band ratio antennas, where band ratio is defined as the ratio of the upper and lower 3dB rolloff frequencies of the radiated pulse. Current systems can achieve band ratios approaching 100 (2 decades of bandwidth) [1]. Through a combination of a non-dispersive transverse electromagnetic (TEM) feed structure and a focused aperture, IRAs act like differentiators for the early-time portion of the waveform. When excited by a fast-rising step, the radiated field closely resembles a narrow impulse. While the nature of the focusing optic and the feed structure do affect the features of the radiated waveform before and after the prompt impulse, the fast part of the radiated signal for a general IRA is [2,3,4]

$$\mathbf{E}_{rad}(r,t) = \frac{\iint_{S_a} \mathbf{E}(x,y)dxdy}{V_0 2\pi rc} \frac{dV(t)}{dt}, \tag{1}$$

$V(t)$ is the applied voltage waveform, V_0 is the peak of the applied voltage waveform, and the surface integral is over the transverse components of the TEM mode in the aperture defined by S_a. The radiated field can also be described in terms of the geometric impedance factor of the TEM transmission line feed defined by

$$f_g = Z_{line}/Z_{med} \tag{2}$$

and the aperture height [5]

$$h_a = -\frac{f_g}{V_0} \iint_{S_a} \mathbf{E}(x,y)dxdy\,. \tag{3}$$

The aperture height is a convenient parameter, because both the transmitted and received peak waveforms can be expressed in terms of h_a as [3]

$$\begin{aligned} E_{rad}(t) &= -\frac{h_a}{2\pi rcf_g}\frac{dV}{dt}, \\ V_{rec}(t) &= -h_a E_{inc}(t) \end{aligned} \tag{4}$$

where E_{rad} and E_{inc} are the magnitudes of the principal component of the radiated or incident field respectively.

I.A. Performance Metrics

A number of metrics have been proposed to compare the performance of antennas operating in the time domain [6,7,8]. The difficulty in comparing performance arises from the non-unique choice of a norm for time domain comparisons. In [7] and [8], performance metrics

are defined in terms of the ∞-norm, or the peak radiated field. Farr and Baum define a power normalized gain

$$G_p = \frac{h_a}{\sqrt{f_g}} \tag{5}$$

that is used to compare the performance of antennas under constant input power conditions, and a voltage normalized gain

$$G_v = \frac{h_a}{f_g} \tag{6}$$

that is used to compare the performance of antennas under constant input voltage conditions. Optimization of the latter quantity typically is accomplished by allowing f_g to go to zero, an impractical scenario that requires infinite input power and results in infinite fields in the aperture [7]. For that reason, the power normalize gain is often a better metric; however, G_p as defined in (5) has units of length, and care must be taken when applying it to an optimization problem in order to make a fair comparison between antennas of different sizes, as G_p can be increased simply by increasing the physical size of the antenna. For example, when optimizing the feed impedance of a lens IRA constrained to fit within a circular aperture of fixed radius, Farr and Baum [9] used G_p to conclude that low-impedance horns were undesirable. This result is true given the imposed constraint, but the result is dominated by the fact that the area of the aperture of low impedance horns that fit inside a circle of fixed radius goes to zero as $Z \to 0$.

Buchenauer, *et al.*, [8] introduced the dimensionless quantity of prompt aperture efficiency defined as

$$\eta_{a.} = \frac{1}{A} f_g \left[\frac{1}{V} \iint_{S_a} E_y(x,y) dx dy \right]^2, \tag{7}$$

where A is the area of the aperture defined by S_a and E_y is the principle component of the electric field in the aperture, taken without loss of generality as being parallel to the y-axis. Because of the area normalization in (7), aperture efficiency is the preferred metric for comparing the inherent performance of classes antennas regardless of physical size. In contrast to the result presented in [9], it was demonstrated in [8] that low impedance horns are actually more aperture efficient than high impedance horns, and they can be used to efficiently fill a given aperture by arraying. Aperture efficiency and power normalized gain are related by

$$\eta_a = {G_p}^2 / A. \tag{8}$$

Regardless of the metric used to compute the optimum, it is clear from (4) – (7) that the optimum antenna for a fixed input impedance (fixed f_g) is the one that maximizes the aperture height.

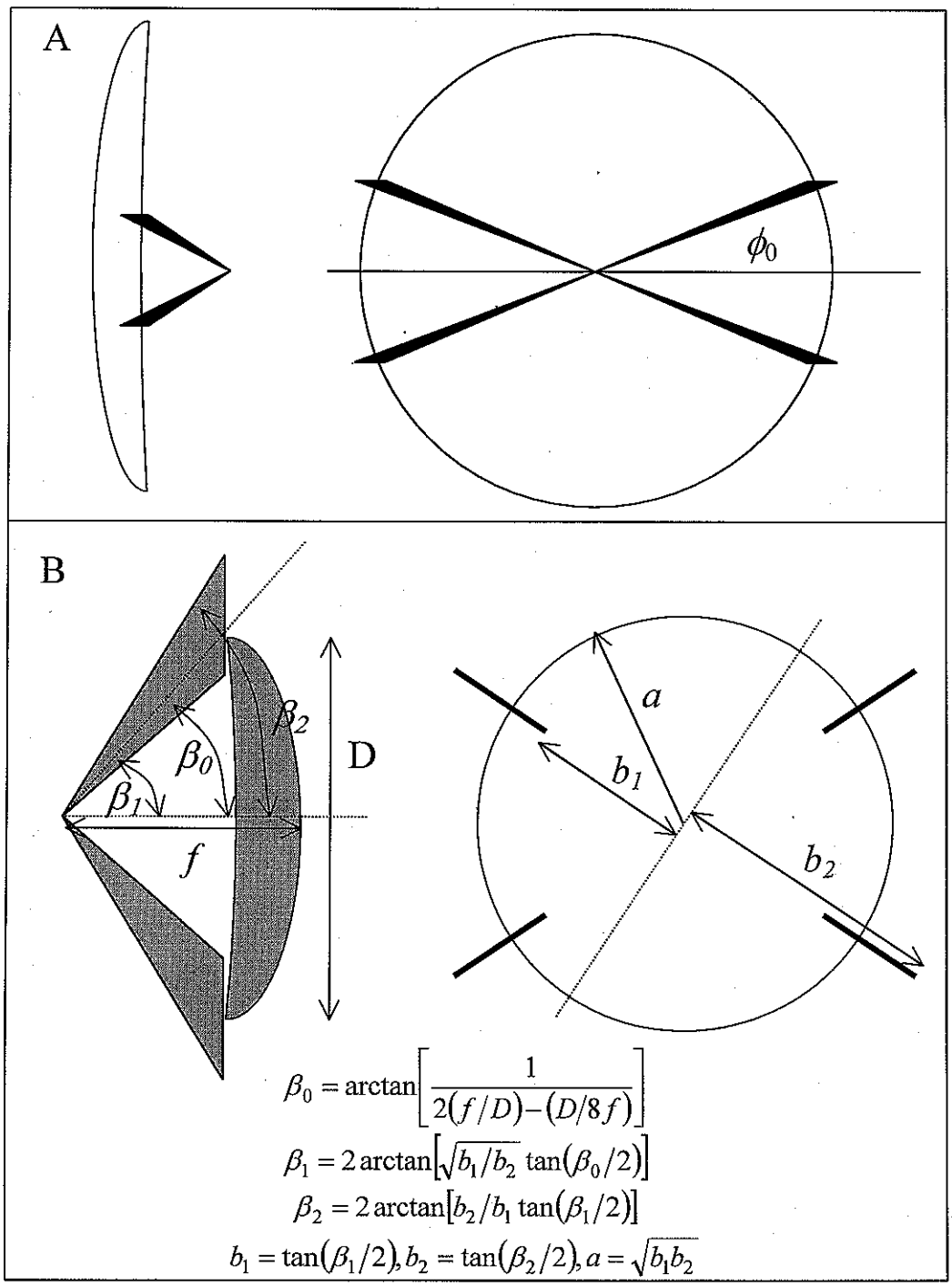

Figure 1: Schematic of the arbitrary crossed coplanar feeds. The feed arms originate from the focal point of the paraboloidal reflector, and the plane of the feed arm makes an angle ϕ_0 with the horizontal symmetry plane. Each pair of feeds is taken to be coplanar, and the intersection point with the circle of symmetry (after sterographic projection) satisfies the self reciprocal condition [1, 10]. Once the focal length f, diameter D, and ϕ_0 are specified and the ratio b_1/b_2 is chosen (equivalent to specifying feed impedance), β_0, β_1, and β_2 can be determined using the relations in the figure.

I.B. Self Reciprocal Apertures

An important class of IRAs is the set of antennas that are fed by self-reciprocal feed structures. Self reciprocal antennas are discussed in [10], and have feed geometries that are unaltered by the reciprocation operation $r \to a^2/r$, where $\mathbf{r} = r\cos\theta\hat{\mathbf{x}} + r\sin\theta\hat{\mathbf{y}}$ is the position vector in the aperture plane (after stereographic projection) and a is the radius of the circle of symmetry. The coplanar feed IRAs discussed in this paper are examples of self-reciprocal apertures, as shown in fig. 1. Self reciprocal apertures have a number of interesting properties, but the most important ones for this study are 1) exactly half of the power on the transmission line propagates outside the circle of symmetry, 2) the total charge on the feed arms inside the circle is equal to the total charge on the feed arms outside the circle of symmetry, and 3) all contiguous points on the circle of symmetry that are not occupied by conductor lie on a single field line.

For the important class of self reciprocal apertures, which are typically confined to focusing the circle of symmetry, the aperture area A is constant for all configurations, and η_a and G_p are equivalent metrics. Aperture efficiency will be the parameter used in this study to optimize the feed configuration in crossed coplanar fed IRAs, primarily because of its dimensionless property and ready interpretation [8].

I.C. Reflector IRAs with Crossed Coplanar Feeds

One of the most common types of IRAs used is the reflector IRA with two pairs of perpendicularly crossed, coplanar feeds [1] ($\phi_0 = 45°$ in fig. 1). Because of the symmetry of the system, the field distribution, feed impedance, and aperture height of this type of antenna can be calculated analytically [2]. While there is no additional complexity associated with making a more general IRA with feed arms that are not oriented at right angles, the only analysis of crossed coplanar fed IRAs whose arms make an arbitrary angle ϕ_0 with respect to the ground plane as shown in fig. 1 was performed by Baum [11] for the high-impedance limit of a wire-fed IRA. In Section II, the TEM mode for the arbitrary coplanar structure is computed numerically using a finite element method code. In Section III, the important design parameters of feed impedance, aperture height, and aperture efficiency are calculated. Section IV contains a discussion of the results and implications of optimizing various features of the antenna, and Section V contains an example of how to use the results in this paper to design a specific system. Conclusions are drawn in Section VI.

II. Computation of the TEM Mode Distribution

It is well known that the field distribution of the TEM mode on a multi-conductor transmission line can be computed as the gradient of a scalar potential that satisfies the Laplace equation [12]. For many classes of feeds, the potential can be calculated using a combination of the stereographic projection and conformal transformations [13]. However, for arbitrary geometries, the conformal map may not exist in closed form. In this study, it is assumed that the stereographic projection has already been carried out, and the conically symmetric feed structure has been transformed to a longitudinally symmetric structure as discussed in [14]. The important properties of the stereographic projection for this class of antennas are summarized in fig. 1 and discussed in greater detail in [14].

The asymmetrically crossed coplanar feed structure depicted in fig. 1 can be described in terms of successive conformal mappings, but the Schwartz-Christoffel transformation integrals for the asymmetric cases $(\phi_0 \neq 45°)$ have not been performed analytically. When the analytic form of the conformal transformation is not known, a numerical approximation can be obtained by employing a Laplace equation solver such as the method of moments or finite element method (FEM). The properties of self-reciprocal symmetry discussed in section *I.B.* above make the geometry depicted in fig. 1 ideally suited to analysis by the FEM. After numerical calculation of the fields, the integrals in (1) – (7) can be evaluated directly or by casting the aperture integral into one of the alternate contour integral forms presented in [5].

The FEM requires a closed computational domain, so it is not always straight-forward to calculate open-mode problems using FEM. The complex potential distribution on a TEM transmission line is an example of an open mode problem, but the reflection symmetries at the $x = 0$ and $y = 0$ planes and the reciprocation symmetry on the circle of radius a shown in fig. 1 allow the geometry to be bounded by perfectly electrically conducting (PEC) $(x = 0)$ and perfectly magnetically conducting (PMC) $(x = 0; r = a)$ surfaces. The symmetry planes also allow the structure to be modeled by considering only one quadrant of the antenna.

The FEM was employed in this study using the Matlab (ver. 5.3) Partial Differential Equations Toolbox (ver 1.0), which was designed to solve 2-dimensional vector and scalar differential equations numerically. The electrode was positioned at an arbitrary position ϕ_0 from the x-axis and held at constant electric potential. The PDE toolbox required the electrode to have finite thickness, and past experience has shown that then the ratio of plate thickness to the next smallest dimension (either separation or width) was less than $1:60$, the field distribution was very close to the theoretical zero-thickness plate result [8,15]. The FEM mesh was composed of linear, triangular elements, and was generated automatically by the PDE toolbox. After computation of a solution to the Laplace equation, the mesh was adaptively refined by subdividing elements where the gradient varies most rapidly in order to better approximate the local electric field near the plate edges.

II.A. Validation of Modeling Method

When $\phi_0 = 45°$, the two crossed pairs of coplanar feeds are perpendicular to each other, and the presence of the second set of electrodes does not alter the fields that are due to the first set alone. For a single pair of electrodes, the complex potential is given by the conformal transformation

$$z(w) = jm^{1/4}\,\mathrm{sn}(w \mid m), \quad z = x + iy;\ w = u + iv \tag{9}$$

where sn($w|m$) is a Jacobian elliptic function [16] and m is the parameter of the elliptic function. In (9), u gives the electric potential and v gives the magnetic potential (or electric field lines). The product of the short and long radii of the electrode is fixed by the self-reciprocal symmetry condition to be $b_1 b_2 = a^2$ [10], and the parameter of the elliptic function is given as $m = (b_1/b_2)^2$. The field distribution can be computed analytically by superposing the fields given by (9) for the two sets of feed arms taken one at a time [2,3]. The feed impedance and aperture heights of the 4-arm IRA are [7]

$$f_g = \frac{K(m)}{2K(1-m)} \tag{10}$$

$$h_a = \frac{\pi m^{-1/4}}{2\sqrt{2}K(1-m)}\left[1 - \frac{2}{\pi}\arcsin\left(\frac{\left(1-m^{1/2}\right)^2}{1-m}\right)\right]. \tag{11}$$

This case can be used as a validation tool for the FEM modeling method. Furthermore, the performance of the adaptive mesh refinement described above can be evaluated, and a stopping criterion can be established for the general case where the analytic solution is not known.

The results of the numerical calculations for the case of $\phi_0 = 45°$, $b_1/a = 0.5$ are shown in figure 2. The diagnostic quantity that was used for the stopping condition in the following sections was the geometric impedance factor f_g. The error in the calculated value for f_g relative to the theoretical value of $f_g = 0.285$ as a function of iteration number is shown in panel 2A, and the number of elements as a function of iteration number is shown in panel 2B. The fractional change in the calculated f_g is shown as a function of iteration number in panel 2C. As can be seen from the figure, the model can get to within ~1% of the theoretical value with a mesh size of ~5000 elements, a number that was fairly typical for most geometries (highly singular geometries where ϕ_0 was close to 0° or 90° or when b_1/a is close to 1 or 0 required more highly refined meshes). Comparing the results presented in panels 2A and 2C led to the development of the following stopping criteria for the adaptive refinements: when three successive mesh refinements had a fractional change of less than 0.003 in the geometric impedance factor, the algorithm terminated. If the number of elements in the mesh exceeded 7500, the adaptive refinement was also stopped regardless of the fractional change in f_g.

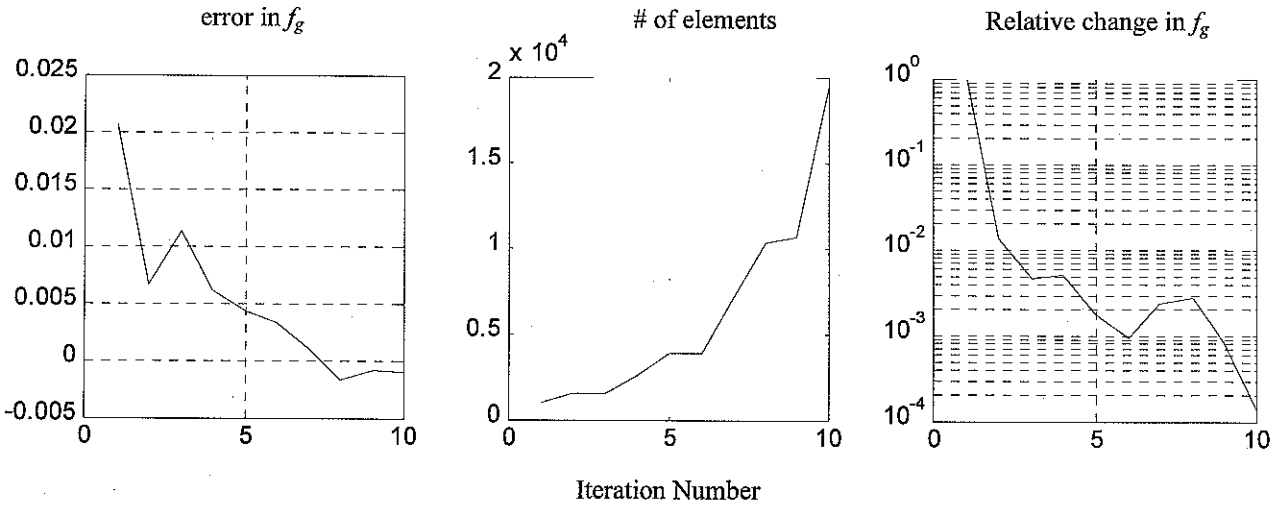

Figure 2: Performance of the FEM modeling tool for the case of $\phi_0 = 45°$ and $b_1/a = 0.5$. The analytic solution for this case is known and $f_g = 0.285$. A. Absolute error in the computed value of f_g as a function of iteration number. B. Number of elements in FEM mesh. C. Relative change in the computed value of f_g as a function of iteration number. These data were used to develop the stopping criterion discussed in the text.

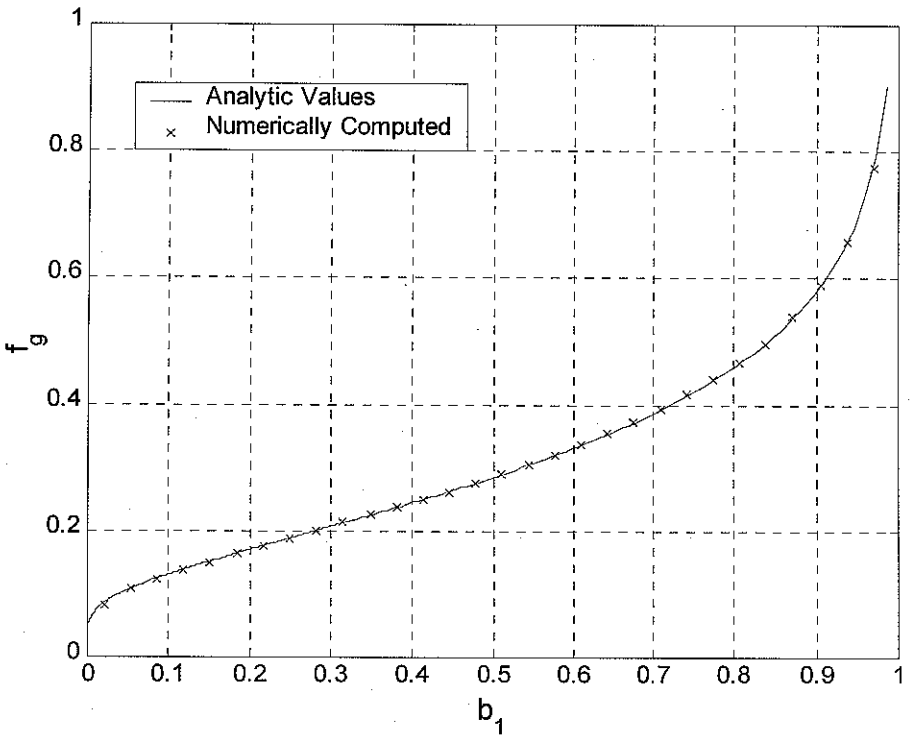

Figure 3: Comparison of numerical computation of geometric impedance factor to the theoretical value predicted by (10). The fit is very close except for the first point $(\phi_0 = 3°)$ where the error is 2.1%. For all other points, the error is less that 0.5%.

Figure 3 presents a comparison of the computed and theoretical values of f_g for $\phi_0 = 45°$ over the range of b_1/a from 0.02 to 0.97. Theoretical values were obtained using (10). The computed values were taken from calculations employing the automatic stopping condition described above (not from the data that went into fig. 2). Except at the lowest impedance $(b_1 = 0.02)$, the error between the calculated and analytic impedance values was less than 0.5%. At the lowest impedance, the error was 2.1%. Figure 4 presents a comparison between the computed and analytic value for the aperture height. Analytic values were obtained using (11). The error at the lowest impedance was 2.1%, but for all other points the error was 1.2% or less.

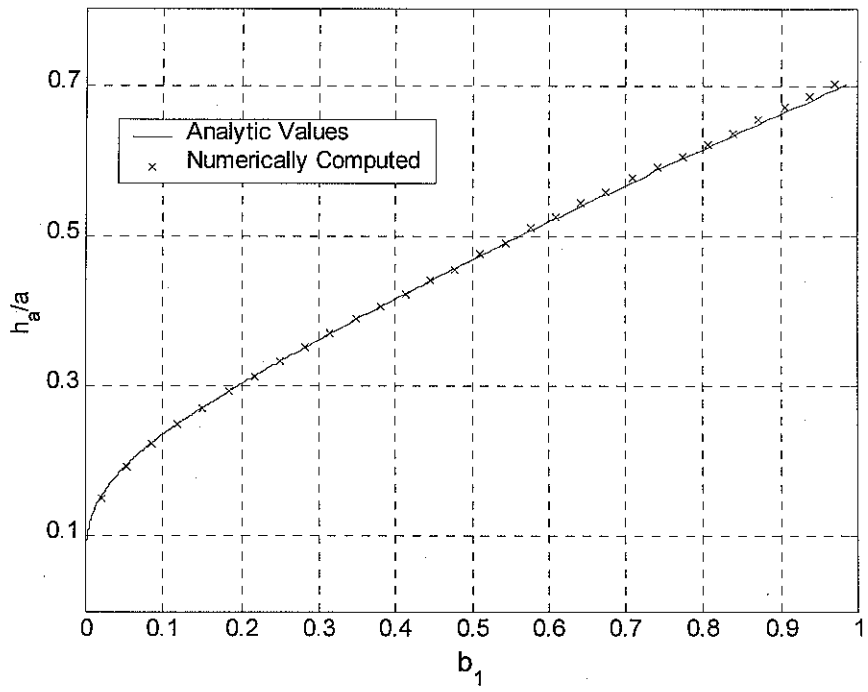

Figure 4: Comparison of numerically computed values of aperture height to the theoretical values predicted by (11). The fit for aperture height is not as good as for the impedance, however, the error is less that 1.5% for all points except for the first $(\phi_0 = 3°)$.

III. Calculation of Antenna Design Parameters

Using the FEM method described in the previous section, the feed impedance, aperture height, and aperture efficiency were calculated at values of ϕ_0 ranging from 3° to 87° and at values of b_1/a ranging from 0.02 to 0.97.

III.A. Feed Impedance

Figure 5 presents a surface plot of the transmission line impedance (assuming free space, $Z_{line} \cong f_g \cdot 120\pi$) as a function of b_1 and ϕ_0. Figure 6 presents curves of f_g -vs- b_1 for several values of ϕ_0 , and fig. 7 presents the value of b_1 as a function of ϕ_0 to achieve popular values of the feed impedance. As expected, $Z_{line} \to 0$ as $b_1 \to 0$ (limit as the spacing between the electrodes goes to zero) and $Z_{line} \to \infty$ as $b_1/a \to 1$ (limit as the electrodes approach infinitesimal wires). The family of curves in fig. 6 has been fitted to the functional form

$$f_g = \frac{A(\phi_0)}{\ln(m) + B(\phi_0)} + C(\phi_0)\ln(1-m) + D(\phi_0)m, \tag{12}$$

where m is given in [7]. The values of the coefficients A, B, C, and D are tabulated for the values of ϕ_0 investigated in this study in appendix 1. The sum of (12) was obtained by analyzing the solution for $\phi_0 = 45°$. The first term is the low-impedance limiting form, the second term is the high impedance limit. The third term represents the error due to the addition of the two asymptotic solutions. Because the actual form of f_g is expected to be given in terms of elliptic integrals and elliptic functions (as in (10) for the $\phi_0 = 45°$ case), the coefficients in (12) do not have a convenient representation in terms of elementary function of ϕ_0. The tabulated values are included for completeness, but estimates for the appropriate value of b_1 for a particular ϕ_0 can be obtained to within 3% by interpolating between the curves presented in fig. 6.

III.B. Aperture Height

Figure 8 presents a surface plot of aperture height as a function of b_1 and ϕ_0. Figure 9 presents curves of h_a -vs- b_1 for several values of ϕ_0. Figure 10 presents the aperture height as a function of ϕ_0 for popular values of the feed impedance. As $b_1 \to a$, $h_a \to a\sin\phi_0$, which is one-half of the mean charge separation for a four-wire transmission line [5]. As $b_1 \to 0$, $h_a \to 0$. The family of curves in fig. 9 is fit by the functional form

$$h_a = \alpha(\phi_0)b_1 + \beta(\phi_0) + \exp(\gamma(\phi_0)b_1 + \delta(\phi_0)). \tag{13}$$

The tabulated values of α, β, γ, and δ are given in appendix 1. The form given in (13) is valid only over the range $0.03 \le b_1/a \le 1$, and strictly *does not fit* the solution as $b_1 \to 0$.

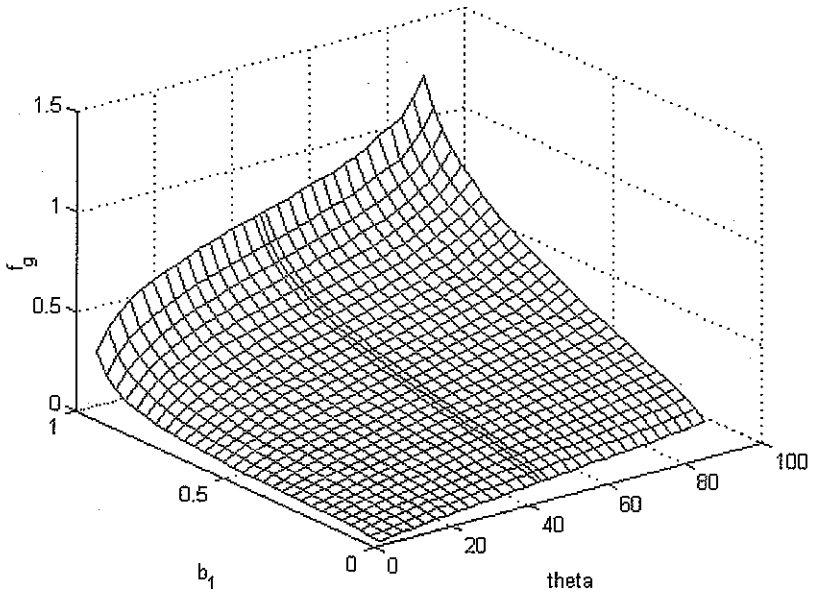

Figure 5: Mesh plot of the geometric impedance factor f_g as a function of b_1 and ϕ_0. These values of impedance were calculated using the FEM technique described in section II.

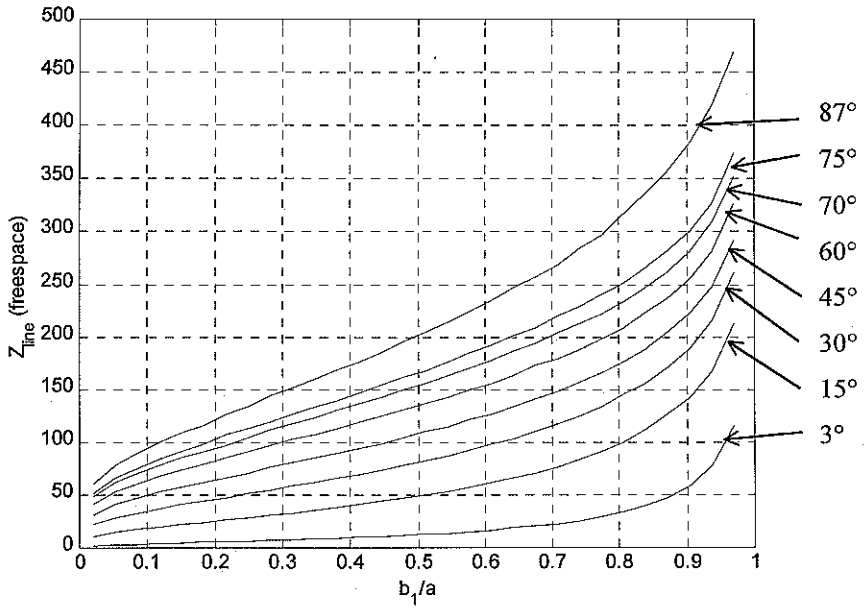

Figure 6: Plots of free space line impedance $\left(f_g \cdot 120\pi\right)$ as a function of b_1/a for a number of values of ϕ_0. For a particular value of ϕ_0, the impedance increases monotonically with b_1/a, and for a particular value of b_1/a, the impedance increases monotonically with ϕ_0.

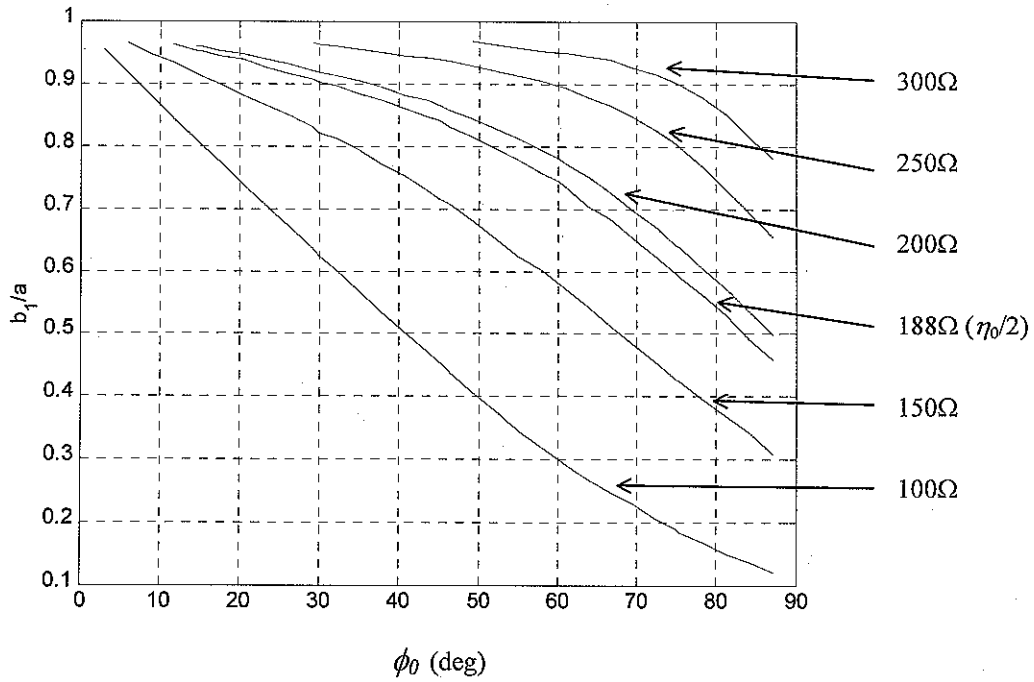

Figure 7: Plate widths as a function of ϕ_0 to obtain popular values of feed impedance. To find the corresponding angular widths for the feed arms of an IRA, use the relations in fig. 1.

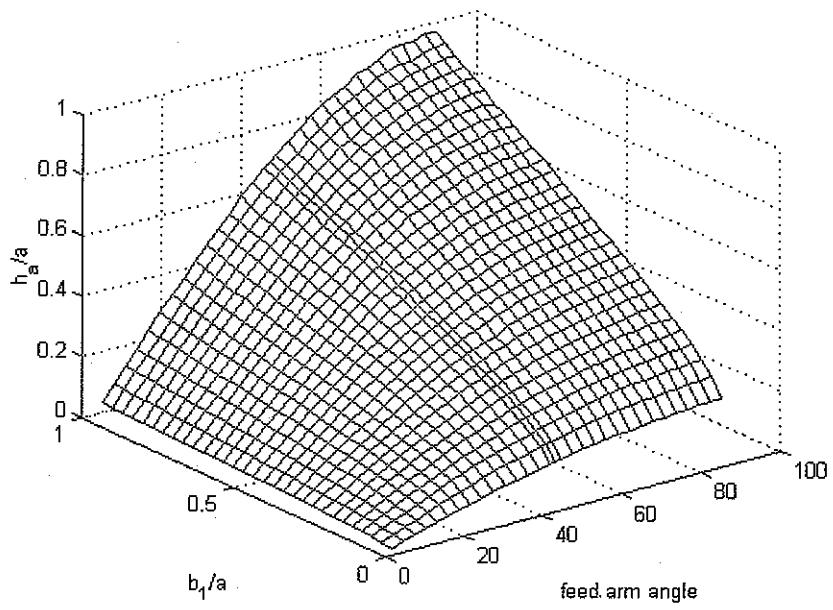

Figure 8: Mesh plot of the aperture height. As $b_1 \to 0$, the electrodes get closer together and the mean charge separation goes to 0. As $b_1 \to a$, the electrodes approach thin wires, and the mean charge separation is equal to $2a\sin\phi_0$.

III.C. Aperture Efficiency

Figure 11 presents a surface plot of aperture efficiency as a function of b_1/a and ϕ_0, and fig. 12 presents curves of η_a-vs- b_1/a for several values of ϕ_0. It is clear from figs. 11 and 12 that there is a particular pair of ϕ_0 and b_1/a that produces the maximum aperture efficiency. The maximum value is $\eta_a = 0.35$, and it occurs at $\phi_0 = 70°, b_1/a = 0.84$. Figs. 11 and 12 show that $\eta_a \to 0$ as $b_1 \to 0, b_1 \to a$ as demonstrated in [8]. Fits for these curves can be obtained by substituting (12) and (13) into (5) and (8).

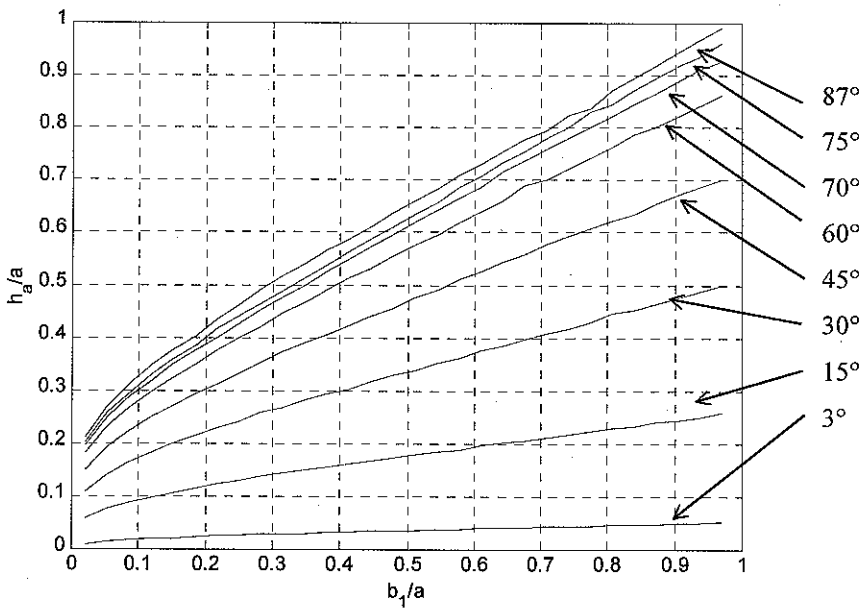

Figure 9: Plots of the aperture height as a function of b_1/a for several values of ϕ_0. The values of ϕ_0 plotted are the same as those in fig. 6 (moving up the page).

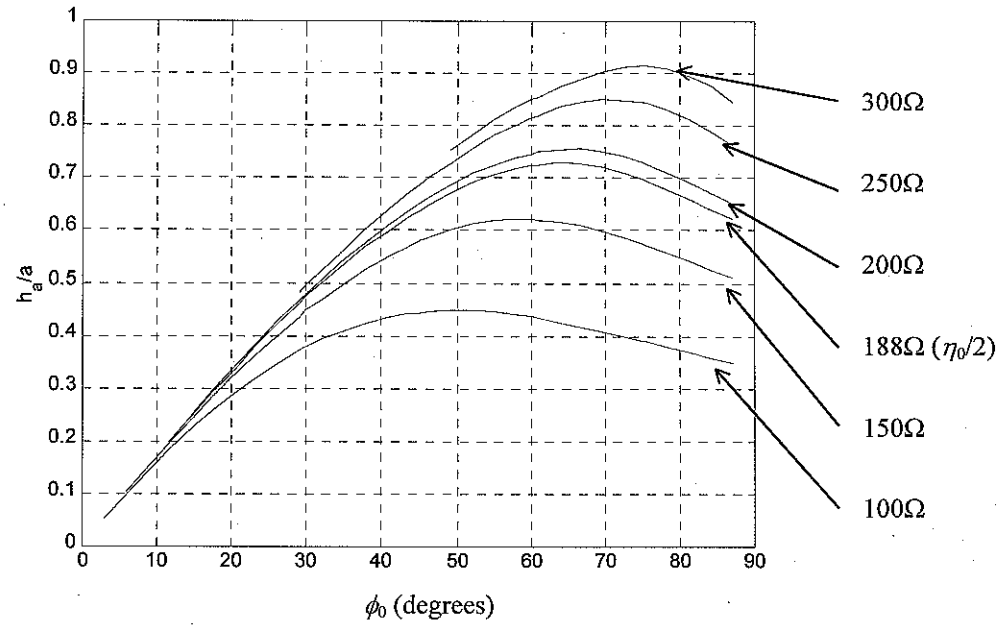

Figure 10: Normalized aperture height as a function of feed arm angle ϕ_0.

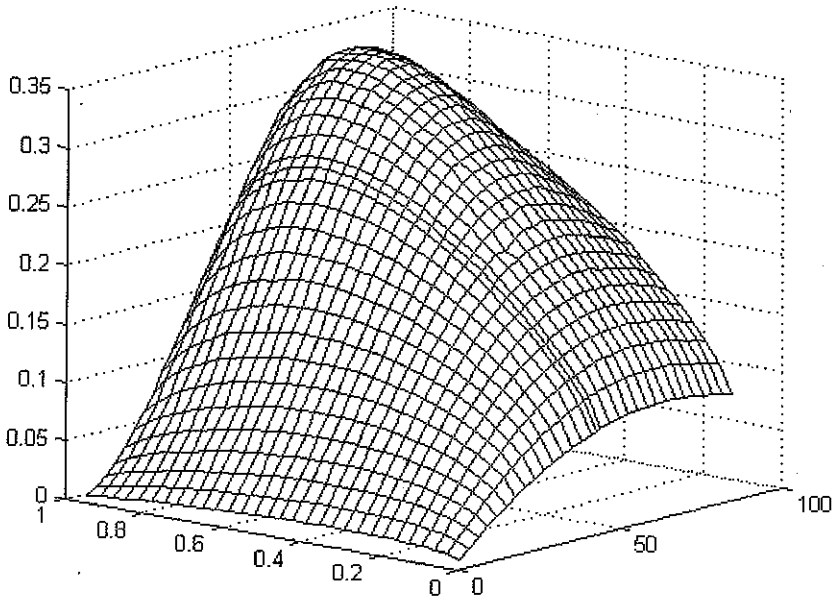

Figure 11: Mesh plot of aperture efficiency as a function of b_1/a and ϕ_0. There is a clear maximum at $\phi_0 = 70°$ and $b_1/a = 0.84$. The value of f_g at this point is 0.65 (247Ω in free space).

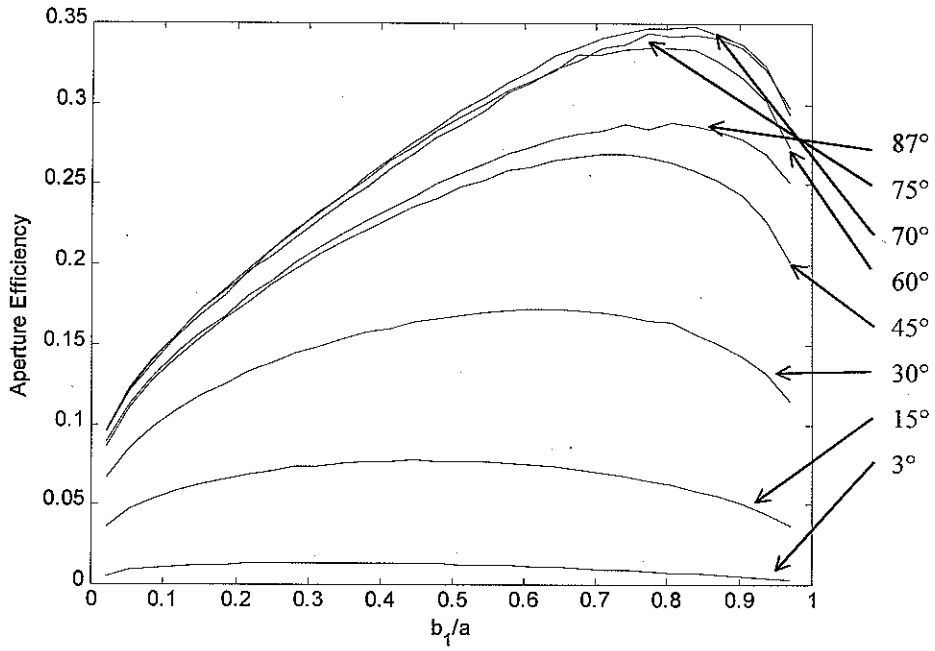

Figure 12: Plots of η_a as a function of b_1/a for several values of ϕ_0. Note that the efficiency is *higher* for the $\phi_0 = 72.5°$ curve than for the $\phi_0 = 87°$ curve.

IV. Discussion

The data presented in figs. 5 - 12 provide all of the information needed to design an antenna wth a particular aperture efficiency, feed impedance, or feed arm angle ϕ_0. However, if the information contained in figs. 6 and 12 is combined, curves of η_a -vs- f_g can be plotted for distinct values of ϕ_0 as is done in fig. 13.

Analysis of fig. 13 provides two interesting results. First, for any particular value of feed impedance, there is a unique geometry that provides the optimum aperture efficiency. The curves in fig. 13 can be used as a design tool to select a particular feed geometry to match the impedance of an individual source. Second, it is clear from the figure that as ϕ_0 increases, the optimum aperture efficiency occurs at higher and higher impedances. The peak value of the aperture efficiency for each ϕ_0 is plotted in fig. 14, and the feed impedance corresponding to this peak is plotted as a function of ϕ_0 in fig. 15. The relationship between optimum feed impedance and ϕ_0 appears to be linear so the data points were fit using a constrained least squares linear regression (setting the intercept to 0). The equation for the line in fig. 15 is

$$\phi_{0,opt} = 1.9234 \frac{Z_{line}}{120\pi}, \tag{14}$$

assuming that the medium is free space. This linear relationship between optimum feed impedance and ϕ_0 was unexpected, and if closed form expressions for the conformal mapping can be obtained, they might provide some physical understanding of the interaction between feed arm angle, extent of the electrodes, and aperture efficiency. It is worth noting that (14) predicts an optimum impedance of 307 Ω for the case of $\phi_0 = 90°$ when the two pairs of crossed coplanar feeds are at the same location, corresponding to the case of a single pair of coplanar feeds. This geometry was optimized by Farr and Baum in [7], and the optimum impedance was found analytically to be 302 Ω, a difference of less than 2%.

In this paper, the optimization was considered for the aperture efficiency (or equivalently, the power normalized gain of [7]). However, for many UWB systems, the quantity that should be maximized is the prompt radiated field, which scales like h_a / f_g , or the voltage normalized gain (G_v) of [7]. As mentioned in the introduction and found in [7], the voltage normalized gain is optimized by allowing $f_g \to 0$. Not only is this impractical for current-flow reasons (since current on the antenna goes like f_g^{-1}), but the wide feed arms needed to obtain low impedances may be expected to significantly enhance feed blockage [17]. However, the importance of G_v for maximizing the radiated field should not be overlooked in designing a system, and hence the value of G_v (normalized to the aperture radius a) is plotted as a function of ϕ_0 in fig. 16 for several important values of the feed impedance.

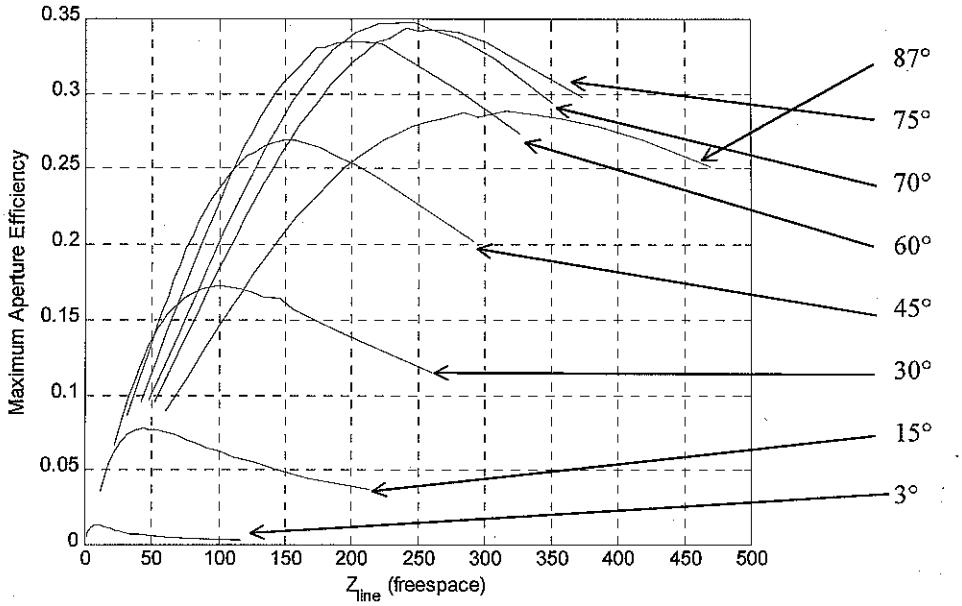

Figure 13: Plots of aperture efficiency as a function of feed impedance (in free space). As ϕ_0 increases, the curves shift to the right. The graph shows that the optimum feed impedance increases monotonically with ϕ_0.

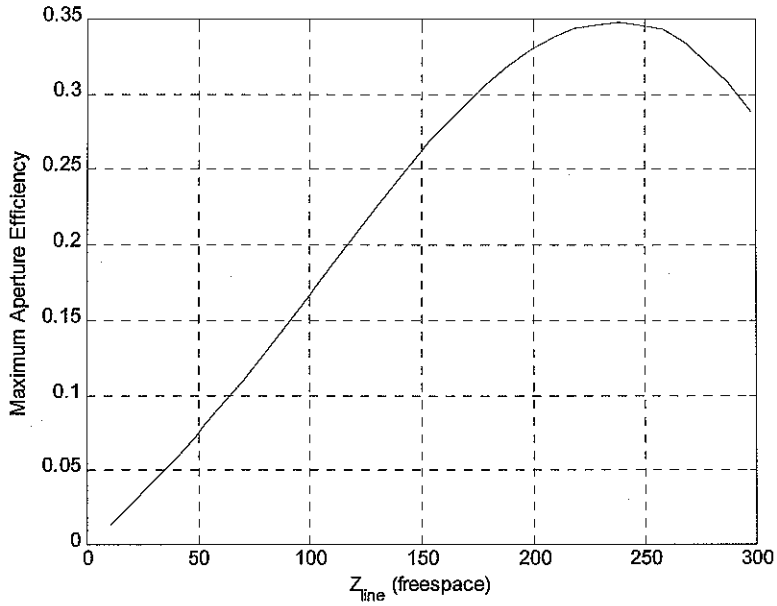

Figure 14: Optimum aperture efficiency as a function of feed impedance. The peak aperture efficiency is 35% at $Z_{line} = 247\Omega$. The optimum angle ϕ_0 for each value of Z_{line} can be obtained from fig. 15 or Eq. 14.

The optimization reported here was for the 4-arm IRA, but there is nothing preventing a similar analysis of *N*-arm IRAs. The optimum aperture efficiency for the 2-arm IRA can be computed using the results from [7] and is 27%. The optimum aperture efficiency for the 4-arm case considered here is 35%. Intuitively, the addition of *non-blocking* feed arms will continue to optimize the aperture efficiency. This is true because additional feeds cause the field distribution in the aperture to be more uniform, hence increasing aperture efficiency. It was shown in [8] that $\eta_{AP} \leq 50\%$ for all self-reciprocal antennas that focus the circle of symmetry, and it was demonstrated in [18] that the circular conical feed structure depicted in fig. 17 with $\phi = 45°$ has the most uniform field distribution in the aperture. It can therefore be concluded that the optimum 4-arm IRA with $\phi_0 = 70°$, $b_1/a = 0.84$, and $f_g = 0.65$ is the one that most closely approximates the geometry depicted in fig. 17. Furthermore, if only the *prompt* signal is considered, the addition of more non-blocking feed arms will make a better approximation to the geometry in fig. 17, further improving the aperture efficiency. However, the late-time field will be pulled down more rapidly as more feed arms are added, affecting the nature of the radiated pulse, even in the absence of feed blockage.

The analysis presented in this study assumed *no feed blockage* by the coplanar feed lines. This assumption corresponds to the geometric optics analysis that is typically used for IRAs. The presence of large metallic plates in the aperture might be expected to perturb the aperture distribution, thereby reducing the aperture efficiency below that which is predicted by the geometric optics analysis. Quantification of the effect of aperture blockage in coplanar-plate fed IRAs is an issue that merits further investigation.

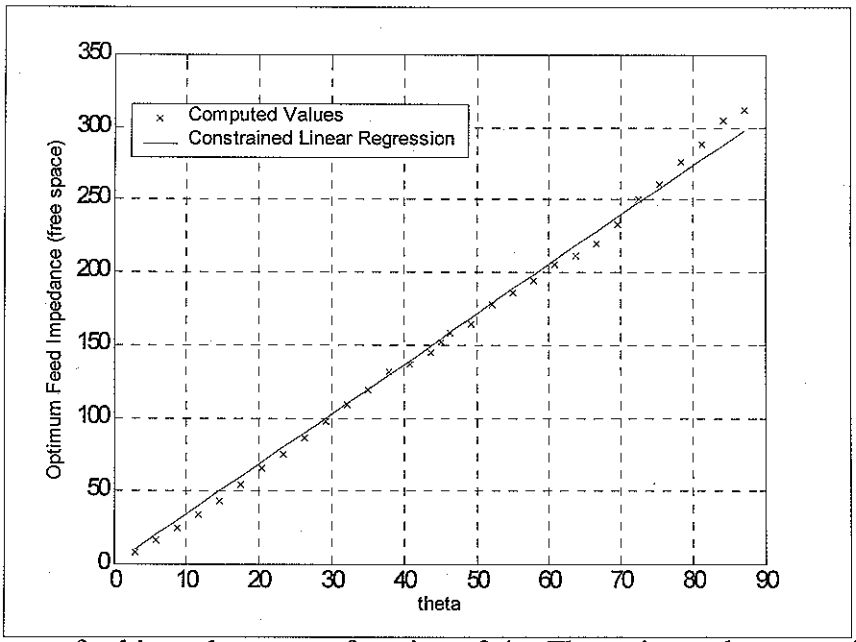

Figure 15: Optimum feed impedance as a function of ϕ_0. The staircased nature of the data is due to similarities in the progression of the adaptive refinement method and stopping strategies between similar geometries. The linear regression was a slope fit only, as the line was constrained to pass thought the origin. Note that the optimum angle for impedances of 100Ω, 150Ω, 200Ω, and 250Ω are approximately 30°, 45°, 60°, and 75°, respectively.

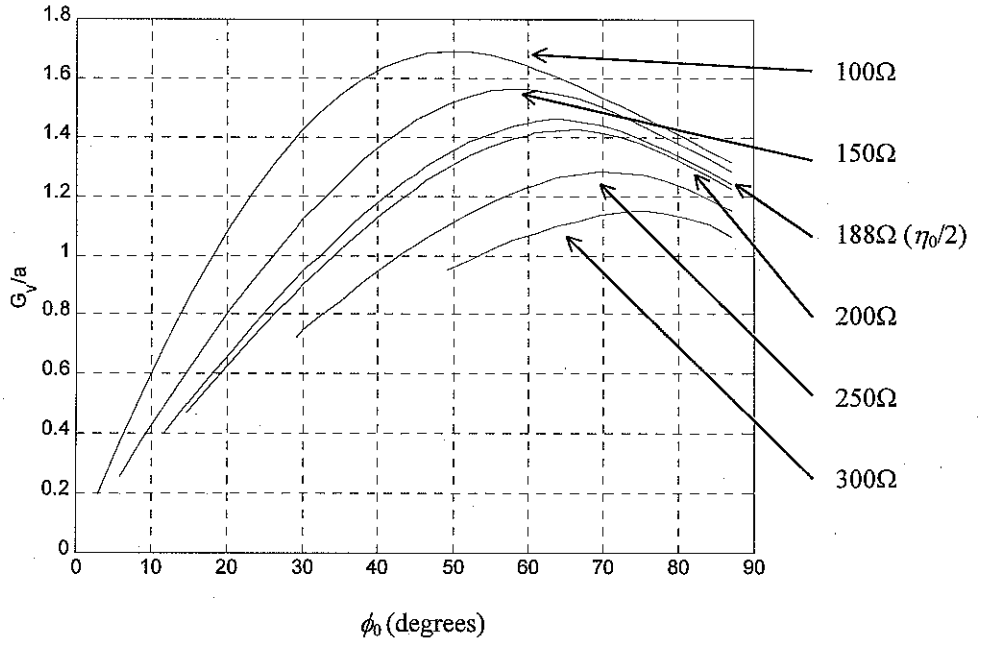

Figure 16: Voltage normalized gain as a function of feed arm angle for popular values of feed impedance, assuming the feed line is in free space. The lower the feed impedance, the higher G_v, but this enhancement may be offset by increased feed blockage at lower impedances.

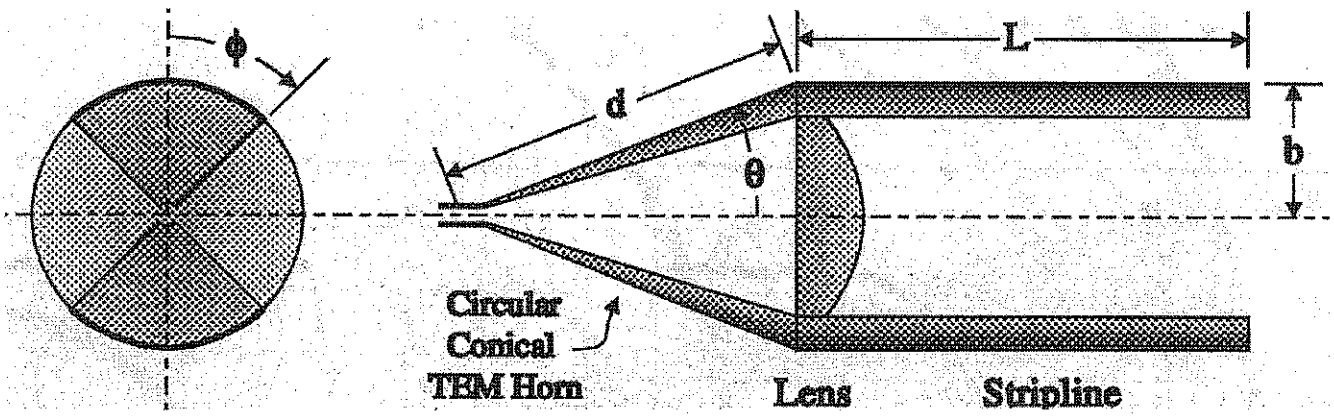

Figure 17: Circular-Conical TEM horn-fed lens IRA. The antenna depicted above is configured with a stripline extension to enhance the late-time response. The 90° section $(\phi = 45°)$ has been shown by Liu [18] to be the optimum geometry for self-reciprocal feed structures. The optimum configuration for the 4-arm IRA is that which most closely approximates the

V. Example Antenna Design Calculation

In this section, a brief example antenna design is performed which will illustrate how to use the data presented in this report. It is assumed that an antenna input impedance of 200Ω $\left(f_g = 0.5305\right)$has been specified due to other considerations in the system. Furthermore, the f/D ratio of the dish has been specified as 0.35.

A. *Identify the angle ϕ_0 corresponding to the optimum configuration for that impedance*
Using either (14) or fig. 15, the optimum feed arm angle is approximately 60° (58.4°).

B. *For the angle $\phi_0 = 58.4°$, estimate the value of b_1/a that gives 200Ω*
Using fig. 6, $b_1/a \approx 0.78$. Equivalently, the curve-fit values in Appendix 1 could be used to plot f_g as a function of b_1 for the appropriate value of ϕ_0.

C. *Estimate the aperture height and aperture efficiency of the antenna*
Using fig. 14, the optimum aperture efficiency for a 200Ω feed is ~33%. The aperture height (normalized to the radius) can be determined using fig. 9 and is ~0.75

D. *Determine the angular extent of the feed plates*
Using the relations in fig. 1 [14],

$$\beta_0 = \arctan\left[\frac{1}{2(f/D) - \frac{1}{8(f/D)}}\right] = 71°$$

$$\beta_1 = 2\arctan\left[\frac{b_1}{a}\tan(\beta_0/2)\right] = 58°$$

$$\beta_2 = 2\arctan\left[\left(\frac{a}{b_1}\right)^2 \tan(\beta_1/2)\right] = 85°$$

VI. Conclusions

The study described in this paper has provided three principle results. First, the entire design space for reflector IRAs fed by crossed coplanar feeds with reflection symmetry has been sampled. Curves are presented in figs. 6, 9, and 12, with corresponding empirical fits in (12) and (13), that allow ready prediction of feed impedance, aperture height, and aperture efficiency as a function of the geometric parameters of the antenna. These relationships provide more flexibility in IRA design beyond what was possible using configurations with known analytic solutions [7]. Second, the data presented in this paper allows the optimization of the aperture efficiency for any value of the geomterical properties. It has been shown that a distinct optimum exists for any feed arm angle ϕ_0 and that an absolute optimum configuration exists at $\phi_0 = 70°$, $b_1/a = 0.84$, and $f_g = 0.65$ (247 Ω in free space). Finally, the results presented in figs. 13 and 15 show that for any specific value of feed impedance, there is a unique optimum configuration that will maximize aperture efficiency. The feed arm angle is linearly related to the desired impedance by (14). This is important in that once the input impedance of the antenna is specified, the antenna can be optimized without impacting upstream components of the system by selecting the appropriate values of ϕ_0 and b_1/a presented in this paper.

The method used in this report are general in that they can be applied to any focused aperture system to calculate feed impedance and aperture height (and hence any of the performance metrics described above). While best suited to the analysis of self reciprocal apertures, iterative boundary condition methods have been developed that allow computation of open TEM modes [15, 8]. The method can be easily modified to include the effects of aperture blockage in the evaluation of (3), allowing analysis of geometries for the feed arms that are not coplanar plates, including circular-cross-sectioned feed arms, curved plates, or other arbitrary configurations.

Appendix 1 - Tabulation of Curve Fit Parameters

Table A1 contains the fitted values of the parameters in (12) and (13). The fitting was performed using a nonlinear-least-squares curve fitting algorithm employing the conjugate gradient search strategy. No global optimization was performed, and other functional forms may fit the data better (as should be expected because the functional forms in (12) and (13) are not correct for the $\phi_0 = 45°$ case). To aid in convergence, the parameters for a neighboring value of θ were used as the starting point for the fitting for each ϕ_0. The fitting process was initialized by considering the low- and high-impedance limit for the $\phi_0 = 45°$ case. The fitted functions can be used to estimate the aperture efficiency to within 1% of absolute efficiency (typically <5% relative).

ϕ_0 (°)	α	β	γ	δ	A	B	C	D
3.00	0.0316	0.0205	-10.3587	-4.0954	-0.1570	-3.0223	-0.1545	-0.0884
5.90	0.0651	0.0383	-10.2862	-3.8281	-0.2820	-2.8715	-0.1600	-0.0354
8.79	0.0986	0.0557	-10.2364	-3.5305	-0.3917	-2.6058	-0.1593	-0.0145
11.69	0.1316	0.0727	-10.1859	-3.3048	-0.4979	-2.5357	-0.1550	-0.0014
14.59	0.1652	0.0890	-10.1449	-3.1274	-0.5622	-2.0432	-0.1551	-0.0395
17.48	0.1993	0.1042	-10.1147	-3.0004	-0.6512	-2.0004	-0.1506	-0.0483
20.38	0.2340	0.1184	-10.0868	-2.9018	-0.7378	-1.9651	-0.1524	-0.0734
23.28	0.2667	0.1332	-10.0616	-2.7897	-0.8173	-1.9389	-0.1458	-0.0840
26.17	0.3014	0.1458	-10.0247	-2.7246	-0.8974	-1.9260	-0.1494	-0.1124
29.07	0.3326	0.1595	-9.9906	-2.6339	-0.9779	-1.9213	-0.1532	-0.1447
31.97	0.3653	0.1713	-9.9539	-2.5746	-1.0571	-1.9276	-0.1599	-0.1782
34.86	0.3965	0.1830	-9.9202	-2.5201	-1.1280	-1.9170	-0.1532	-0.1900
37.76	0.4288	0.1934	-9.8826	-2.4742	-1.2128	-1.9472	-0.1699	-0.2369
40.66	0.4580	0.2043	-9.8379	-2.4265	-1.2913	-1.9817	-0.1641	-0.2415
43.55	0.4875	0.2129	-9.7751	-2.4090	-1.4053	-2.1955	-0.1669	-0.2208
45.00	0.5019	0.2175	-9.7341	-2.3952	-1.4494	-2.2173	-0.1636	-0.2219
46.45	0.5133	0.2228	-9.6684	-2.3616	-1.5033	-2.2997	-0.1669	-0.2215
49.34	0.5407	0.2308	-9.5886	-2.3413	-1.6441	-2.5710	-0.1684	-0.1935
52.24	0.5689	0.2363	-9.5198	-2.3575	-1.7476	-2.6735	-0.1659	-0.1864
55.14	0.5925	0.2445	-9.3905	-2.3243	-1.8475	-2.7230	-0.1712	-0.2038
58.03	0.6146	0.2499	-9.3366	-2.3315	-1.9553	-2.8292	-0.1728	-0.2017
60.93	0.6318	0.2577	-9.2838	-2.2913	-2.0831	-2.9717	-0.1676	-0.1844
63.83	0.6529	0.2618	-9.2085	-2.3026	-2.1778	-2.9904	-0.1587	-0.1756
66.72	0.6717	0.2641	-9.1689	-2.3354	-2.2700	-2.9855	-0.1701	-0.2067
69.62	0.6878	0.2675	-9.1434	-2.3349	-2.3482	-2.9469	-0.1600	-0.1997
72.52	0.7007	0.2704	-9.1396	-2.3498	-2.4475	-2.9515	-0.1639	-0.2112
75.41	0.7179	0.2702	-9.2836	-2.4160	-2.5470	-2.9435	-0.1657	-0.2119
78.31	0.7172	0.2770	-9.3742	-2.3382	-2.6401	-2.9020	-0.1573	-0.2081
81.21	0.7212	0.2806	-9.9232	-2.3147	-2.7333	-2.8553	-0.1507	-0.1927
84.10	0.7350	0.2772	-12.4472	-2.2886	-2.8639	-2.8983	-0.1517	-0.1472
87.00	0.7247	0.2872	-12.3703	-2.1695	-3.0014	-2.9122	-0.1669	-0.1140

Table A1

References

[1] D. V. Giri and C. E. Baum, "Temporal and Spectral Radiation On Boresight of a Reflector Type of Impulse Radiating antenna" in *Ultra-Wideband, Short Pulse Electromagnetics 3*, C. E. Baum, L. Carin, and A. P. Stone, Eds., pp. 65-72 (Plenum, New York, 1997)

[2] C. E. Baum and E. G. Farr, "Impulse Radiating Antennas" in *Ultra Wideband/Short Pulse Electromagnetics* H. L. Bertoni, C. E. Baum, and L. B. Felson, Eds., pp. 139-147, Plenum Press, New York, 1993

[3] E. G. Farr, C. E. Baum, and C. J. Buchenauer, "Impulse Radiating Antenna, Part II" *Ultra-Wideband, Short-Pulse Electromagnetics 2*, pp. 159-170, Plenum Press, New York, 1995

[4] E. G. Farr and C. E. Baum, "Impulse Radiating Antennas, Part III" in *Ultra-Wideband, Short-Pulse Electromagnetics 3*, C. E. Baum, L. Carin, and A. P. Stone, Eds., pp. 43-56 (Plenum, New York, 1997)

[5] C. E. Baum, "Aperture Efficiencies of IRAs" *Sensor and Simulation Notes* #328, C. E. Baum, Ed., June 1991 (USAF Phillips Lab, Albuquerque, NM)

[6] E. G. Farr and C. E. Baum, "Extending the Definitions of Antenna Gain and Radiation Pattern Into the Time Domain" *Sensor and Simulation Notes* #350, C. E. Baum, Ed., November 1992 (USAF Phillips Lab, Albuquerque, NM)

[7] E. G. Farr and C. E. Baum, "Optimizing the Feed Impedance of Impulse Radiating Antennas Part I: Reflector IRAs" *Sensor and Simulation Notes* #354, C. E. Baum, Ed., January 1993 (USAF Phillips Lab, Albuquerque, NM)

[8] C. J. Buchenauer, J. S. Tyo, and J. S. H. Schoenberg, "Aperture Efficiencies of Impulse Radiating Antennas" *Sensor and Simulation Notes* SSN#421, C. E. Baum, Ed., November 1997 (USAF Research Lab, Albuquerque, NM)

[9] E. G. Farr, "Optimization of the Feed Impedance of Impulse Radiating Antennas, Part II: TEM Horns and Lens IRAs" *Sensor and Simulation Notes* SSN#384, November 1995 (USAF Phillips Lab, Albuquerque, NM)

[10] E. G. Farr and C. E. Baum, "Radiation from Self-Reciprocal Apertures" Chapt. 5 in *Electromagnetic Symmetry*, C. E. Baum and H. N. Kritikos, Eds., Taylor and Francis, Bristol, PA, 1995

[11] C. E. Baum, "Selection of Angles Between Planes of TEM Feed Arms of an IRA" *Sensor and Simulation Notes* #425, August 1998 (USAF Research Lab, Albuquerque, NM)

[12] W. R. Smythe, *Static and Dynamic Electricity, 3rd Edition*, ch. 4, pp. 63-120 (Taylor and Francis, Washington, DC, 1989)

[13] P. Moon and D. E. Spencer, *Field Theory Handbook* (Springer-Verlag, Berlin, 1961)

[14] E. G. Farr and C. E. Baum, "Prepulse Associated with the Feed of an Impulse Radiating Antenna" *Sensor and Simulation Notes* #337, C. E. Baum, Ed., March 1992 (USAF Phillips Lab, Albuquerque, NM)

[15] C. J. Buchenaeur, J. S. Tyo, and J. S. H. Schoenberg, "Antennas And Electric Field Sensors For Ultra Wideband Transient Measurements: Applications And Methods" *Ultra-Wideband, Short-Pulse Electromagnetics III* , C. E. Baum, L. Carin, and A. P. Stone, Eds. Pp. 405-421 (Plenum Press, New York, 1997)

[16] M. Abromowitz and I. A. Stegun, *Handbook of Mathematical Functions* (Dover, New York, 1965)

[17] E. G. Farr, *Personal Communication*, October 1999

[18] T. K. Liu, "Impedances and field districutions of Curved Parallel-Plate Transmission-Line Simulators" *Sensor and Simulation Notes* SSN#170 (USAF Research Lab, Albuquerque, NM, Feb. 1973)